Marine Geology 412 (2019) 37–52

Contents lists available at ScienceDirect

Marine Geology

journal homepage: www.elsevier.com/locate/margo

Morphology and maintenance of steep dunes near dune asymmetry transitional areas on the shallow shelf (Beibu Gulf, northwest South China Sea)

Xiaochuan Ma[a,b,c,*], Jun Yan[a,b,c], Yongdong Song[a], Xiansan Liu[a], Jianxing Zhang[a], Peter A. Traykovski[d]

[a] CAS Key Laboratory of Marine Geology and Environment, Institute of Oceanology, Chinese Academy of Sciences, Qingdao, P. R. China
[b] Laboratory for Marine Geology, Qingdao National Laboratory for Marine Science and Technology, Qingdao, P. R. China
[c] Center for Ocean Mega-Science, Chinese Academy of Sciences, Qingdao, 266071, P. R. China
[d] Applied Ocean Physics and Engineering Department, Woods Hole Oceanographic Institution, Woods Hole, MA, USA

ARTICLE INFO

Editor: Edward Anthony

Keywords:
Steep dunes
Morphology
Maintenance
Flow separation
Beibu Gulf

ABSTRACT

Symmetrical dunes can be found in areas where dune asymmetry changes sense, but in areas where dunes are not expected to be moving the development and maintenance of symmetrical dunes are poorly understood. In the southeastern Beibu Gulf, we have identified five typical dune asymmetry transitions at the depths of shallower than 50 m basing on the latest bathymetric data. Those regions are separated into two classes according to their different shapes and locations. Sand transport directions are deduced by dune migrations between surveys, simulated regional currents, and sand size trends. The two classes of the regions are found to experience opposing net sand transports from the north and south. Around the asymmetry transitions, the dunes have impressive steep sections, relatively symmetrical shapes, and almost straight crests. They have a general Height-Length (H-L) relation: $H = 0.0575 L^{1.0836}$ ($R^2 = 0.834$), which is steeper than dunes in other seas. Some of the dunes have extraordinary large heights exceeding a quarter of water depth, which is attributed to the preserved sand body, bidirectional sand accretion, erosion in troughs, and absence of significant erosion on crests. The steepness and straight crests of dunes adapt to the nearly symmetrical or weak asymmetrical reversing currents, which induce flow separations and reversals on both flanks of the dunes. It also suggests that dunes develop differently under sufficient and limited sand supply. Dunes will gradually grow in size when being continually supplied with sand. However, if sand supply is restricted, dunes may separate or turn into more isolated individuals to sustain the H-L relation. The H-L relation of dunes can be maintained during either growth or separation. Overall, the nearly symmetrical or weak asymmetrical reversing currents maintain the steep shapes of dunes while variations in sand supply affect their sizes. To work out the detailed transports of sediment, future observations of flow structures and related models of such two-sided steep dunes are still required.

1. Introduction

Sand dunes are ubiquitous on shelves (Dalrymple, 1978; Ashley, 1990; Dalrymple and Rhodes, 1995; Anthony and Leth, 2002; Barnard et al., 2006; Van Landeghem et al., 2009a, 2009b; Franzetti et al., 2013) and usually have crests approximately normal to tidal currents. They initially develop from amplitude increases of seabed disturbance caused by interactions between oscillatory currents and the seabed (Hulscher et al., 1993; Hulscher, 1996; Gerkema, 2000; Komarova and Hulscher, 2000; Besio et al., 2003) and subsequently grow to various shapes under the influences of tidal currents, basal topography (Van Landeghem et al., 2009a), surface waves (Van Dijk and Kleinhans, 2005; Walgreen et al., 2002), sediment grain size (Van der Veen et al., 2006), and suspended sediment transport (Besio et al., 2003). Indeed, most sand dunes have asymmetrical sections and inclined stratigraphy under unequal tidal currents (Allen, 1980; Berné et al., 1988, 1993; Lobo et al., 2000; Wynn et al., 2002; Le Bot and Trentesaux, 2004; Ferret et al., 2010) while few of them are trochoidal or relatively symmetrical. In the previous papers, the trochoidal or nearly symmetrical dunes are only reported in several areas, like Gironde estuary (Berné et al., 1993), Juan de Fuca Strait (Mosher and Thomson, 2000), Irish Sea (Van Landeghem et al., 2009a), Gibraltar Strait (Lobo et al.,

* Corresponding author at: Key Laboratory of Marine Geology and Environment, Institute of Oceanology, Chinese Academy of Sciences, Qingdao, P. R. China.
E-mail address: mxch@qdio.ac.cn (X. Ma).

https://doi.org/10.1016/j.margeo.2019.03.006
Received 19 January 2018; Received in revised form 13 February 2019; Accepted 13 March 2019
Available online 15 March 2019

2010), and bay of Fundy (Duffy, 2012; Todd et al., 2014). Different from the asymmetrical dunes whose origin and migration mechanism have been studied extensively (e.g. Németh et al., 2002, 2007; Besio et al., 2004, 2008), the formation of nearly symmetrical dunes are still under debate. Berné et al. (1993) described the symmetrical dunes with a reversal of layer inclination inside in a macro-tidal estuary and inferred them to be triggered by the fortnightly tidal cycle. In Juan de Fuca Strait, some large dunes with steep and relatively symmetrical shapes were interpreted to be associated with the combination of estuarine circulation, tidal forcing, bathymetric control accelerating currents, and material source (Mosher and Thomson, 2000). In contrast, the large nearly symmetrical dunes found in the Irish Sea were interpreted to be relics and ascribed to the post-glacial reversing sediment transports (Van Landeghem et al., 2009a). Moreover, the geometrical characters of this kind of dunes have not been studied quantitatively and the maintenance mechanism is also elusive. It thus requires more studies to look into their morphology, formation mechanism, and related modern/past sand transport process.

In this study, we report the new-found fields of steep and nearly symmetrical dunes in the Beibu Gulf, northwest of the South China Sea. Basing on the latest bathymetric data and high-resolution seismic data, the morphology and internal structure of the dunes are detailedly documented. We evaluate the regional flows and the bedload transports using a Delft3D model and detect the local flows around dune individuals through in-situ measurements. The shape figuration and maintenance mechanism of the dunes are further discussed. The study is organized as follows: Section 2 describes the regional settings. Section 3 is the data acquisition and analysis method. Section 4 documents the results including bedload convergences, dune geometrical characters, and characters of currents and sediments. In Section 5, morphological equilibrium, the origin, and maintaining mechanisms under strong reversing currents are discussed.

2. Regional settings

Our study area is located in the southwest of the Beibu Gulf (Gulf of Tonkin), northwest of the South China Sea. Beibu Gulf is a bay with an open edge in its south and a strait (Qiongzhou Strait) in its northeast connecting the South China Sea (Fig. 1a). The main area of Beibu Gulf was terrestrial during the last glacial maximum, and the coastline turned to be similar to nowadays from about 6 cal. ka BP (Yao et al., 2009). After that, the sea level in the South China Sea has not largely fluctuated and the sea coverage is relatively stable. In the gulf coast, sediment mainly consists of well-sorted sand, fine sediment, and gravel, which could come from coastal erosion, river input, and sediment transport from the open sea (Xu et al., 2010). It is also reported that a sediment transport convergence emerges near the study area (Xu et al., 2010) (Fig. 1b). Field observations have shown that tidal currents are reversing in the study area and the northwards flood currents are larger in deeper areas (Xia et al., 2001). Tidal currents have maximum speeds larger than 0.6 m/s near the bottom (Ma et al., 2014) and larger than 1.0 m/s near the surface (Xia et al., 2001). Also, tropical storms are frequent in most years and can easily produce episodic high-energetic currents and waves (Ma et al., 2013). In the study area, various bedforms including sand waves and sand ridges develop on the seafloor under the tidal currents (Xia et al., 2001; Cao et al., 2006; Ma et al., 2014). Most sand waves and dunes are asymmetrical and mobile, and some dunes can migrate several to tens of meters per year (Ma et al., 2014). Some nearly symmetrical sand dunes were also mentioned in several studies (Xia et al., 2001; Cao et al., 2006; Ma et al., 2013); however, their geometry, mobility, and evolution have not been studied.

3. Data acquisition and analysis

3.1. Data acquisition and sampling

The seafloor of the study area was investigated using a Reson SeaBat 8101 system in 2009 and imaged using the obtained full-coverage high-resolution bathymetric data. In 2010 and 2014, the bathymetry of the particular regions overlapping the survey area of 2009 was further collected through a Sonic 2024 system on board the R/V Kexue-III. During all surveys, a DGPS and an inertial measurement unit (Octans 3000) were used to ensure the positioning accuracy of < 1 m and an attitude accuracy of better than ± 5% (heave) and 0.01° (pitch and roll). The raw data were then processed using CARIS HIPS software package (version 8.1). The bathymetic data were corrected for tidal water level changes using the tide gauge data recorded at the station located about 20 km (straight-line distance) east of the study area (Dongfang, 108°37.5′, 19°6.4′). The local water level was measured in 2016 and used in the raw data processing. The comparison between the measured tidal curve and the tide gauge data shows that they mostly

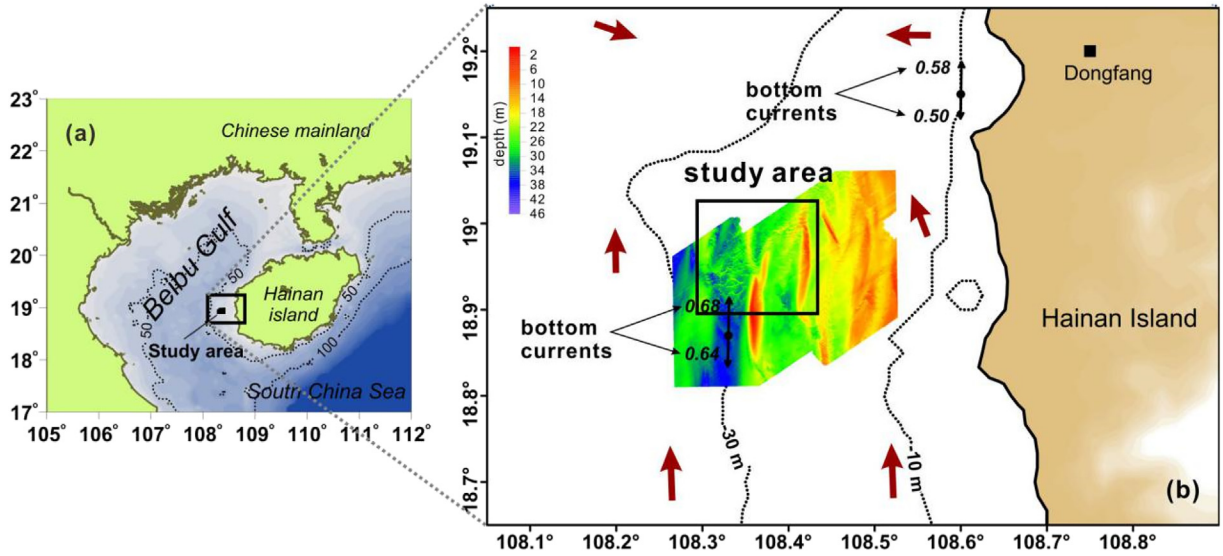

Fig. 1. Location of the study area. The color map shows the bathymetry of the area (b) and the black arrows represent the reversing bottom currents according to Xia et al. (2001). The red arrows denote the sediment transport trend around the study area (Xu et al., 2010). (For interpretation of the references to color in this figure legend, the reader is referred to the web version of this article.)

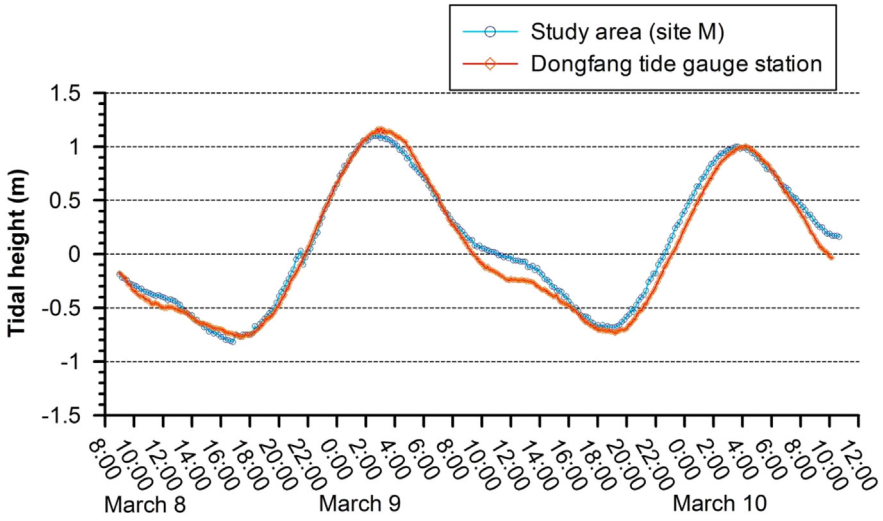

Fig. 2. Comparison between tide gauge data used for tidal correction (orange) and local measured water level in March 2016 (light blue). (For interpretation of the references to color in this figure legend, the reader is referred to the web version of this article.)

match with each other although there are some shifts (lower than 25 cm) during ebb (Fig. 2). This level is comparable with the data described by Schmitt et al. (2008). To image the dune structures, shallow seismic profiles were obtained using a 3.5 kHz GeoAcoustics sub-bottom profiler and gain was manually adjusted in the Sonar Wiz software. Sonar images were also collected by a Klein 3000 sonar system at the same time. During the survey, surface sediments were collected using a van Veen grab sampler and pre-processed in the Lab. The grain size was then obtained through sieving (710, 850, 1000, 1200, 1430, 1700 and 2000 μm) and a Cilas laser granulometry (size smaller than 710 μm) according to Ma et al. (2014). The statistical parameters were also analyzed according to McManus (1988).

3.2. Geometrical analysis

The geometrical characters are measured following the method suggested by Van Landeghem et al. (2012) (Fig. 3). Herein, dune length (L) is uniformly quantified from the adjacent troughs (Knaapen, 2005; Ernstsen et al., 2006; Van Landeghem et al., 2012). Dune height (H) is defined by the distance from crest to basement (adjacent-trough line). Water depth (D) is the sum of dune height and water depth over the crest. Then the correlations between L and H and between H and D are illustrated and also compared to the relations reported in previous studies. The asymmetry parameter is defined as $|L_{stoss}\text{-}L_{lee}|/L$ following the method of Van Landeghem et al. (2012), and the values lower than 0.2 are considered nearly symmetrical and weakly asymmetrical. The migrations of dunes are obtained through the comparisons of typical bathymetric profiles basing on the data at a 2 m per pixel resolution. To look into the accretion and erosion around the dunes, seafloor changes are also investigated by comparing the filtered 20 m-resolution data between 2010 and 2014 in some typical dune fields.

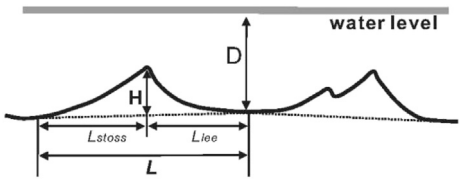

Fig. 3. Definition of geometrical parameters of dunes including height, length, and depth according to Van Landeghem et al. (2012). The asymmetrical parameter is defined as $|L_{stoss}\text{-}L_{lee}|/L$ following the method of Van Landeghem et al. (2012).

3.3. Regional current simulation and local bottom current measurements

We used a Delft 3D model (35-day numerical run) to simulate the regional tidal currents and evaluate the related bedload transports. The model was established for the whole gulf with two open boundaries separately at the Qiongzhou Strait and the south mouth of the bay (Fig. 4). Most bathymetric data of the Beibu Gulf came from ETOPO1 (a resolution of 1 arc-minute) while in the study area the measured high-resolution bathymetry was used. In the model, the whole gulf was covered by the 7.5 km × 5.5 km grids, and the grids of the study area were refined to a mesh resolution of approximately 200 m (Fig. 4). The model was forced by astronomic tidal constituents at the south mouth of the bay and by constant western flows in the Qiongzhou Strait. After the simulation, we verified the modeled principal harmonic constants (K1, O1, M2, S2) using the tide gauge data around the Beibu Gulf (Table 1). The modeled water level and current speed were also verified through the in-situ depth-averaged currents measured with an up-looking ADCP on the seafloor in 2006 (Fig. 4). The modeled currents have clear reactions to the sand ridges and also have good agreements with the dune migrating directions (details can be found in Ma et al., 2018). However, this model cannot capture the flow regimes over dune individuals due to the relatively low grid resolution (200 m). We hence deployed a current meter (ALEC) together with a tide meter at 0.4 m above the seabed in the trough of a dune in Mar. 2016 (site M) to detect the local tidal currents around the dunes. The measured currents were compared to the data collected on a relatively flat floor beside the dunes in Nov. 2014 (site E). The bottom currents were measured for more than two days at both sites. The threshold speeds of depth-averaged currents for sediment movement initiation are calculated according to Ma et al. (2018) to evaluate the mobility of surface sediment.

$$\theta_{cr} = \frac{0.3}{1 + 1.2D_*} + 0.055(1 - e^{0.02D_*}) \quad (1)$$

$$D_* = [g(s-1)/\nu^2]^{1/3} d_{50} \quad (2)$$

$$\theta_{cr} = \frac{\tau_{cr}}{g\rho(s-1)d_{50}} \quad (3)$$

$$\tau_{cr} = \rho C_D u_{cr}^2 \quad (4)$$

$$s = \rho_s/\rho \quad (5)$$

where θ_{cr} is critical shields number and calculated following the relation of Soulsby and Whitehouse (1997); τ_{cr} is the critical shear stress; g is the gravity acceleration; d_{50} is the median grain size; C_D is the bottom

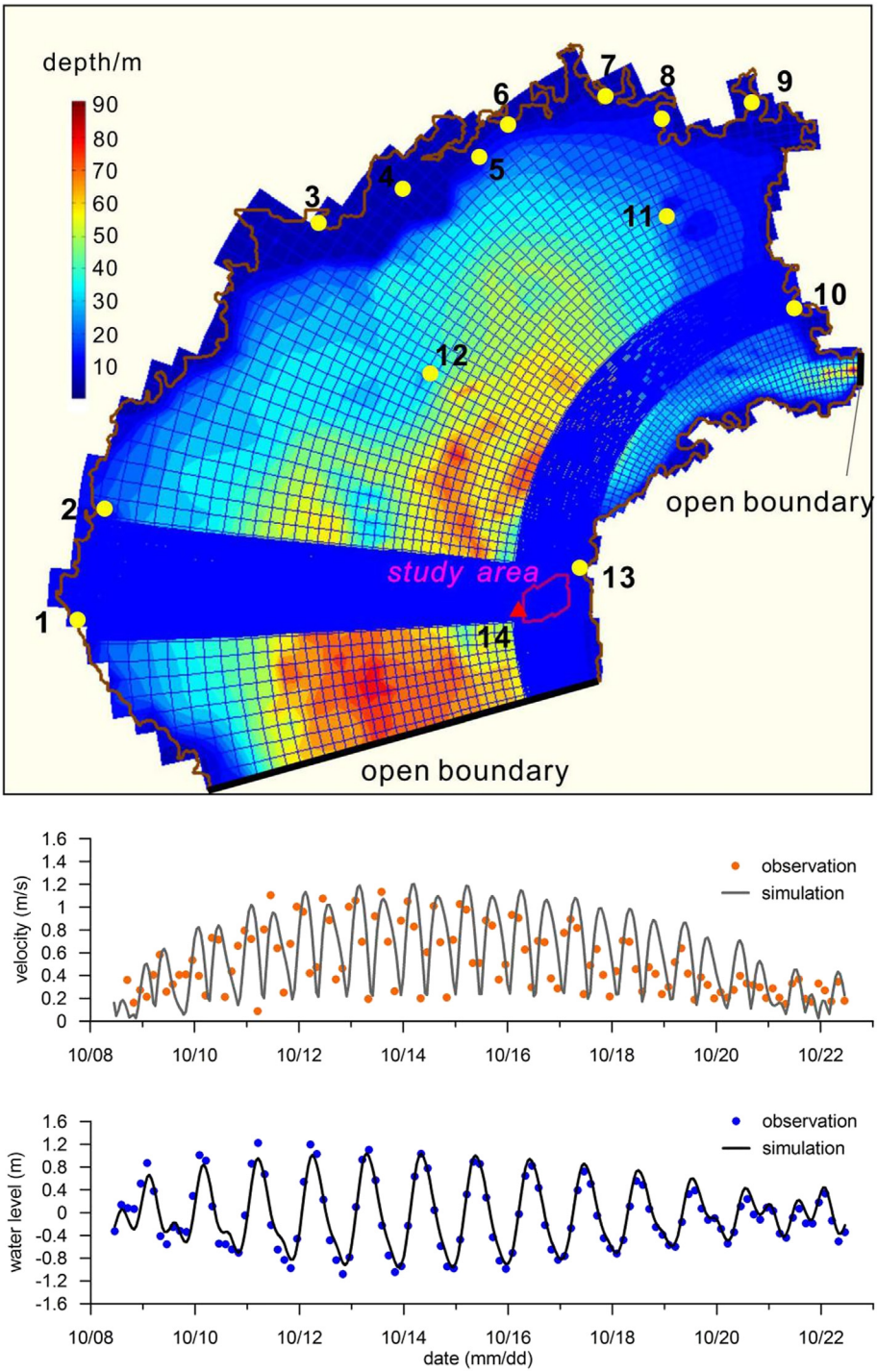

Fig. 4. The grids of model and the locations of sites for model validation (upper panel), in which 1–13 are the tide gauge stations and 14 is the observation site with an up-looking ADCP (modified from Ma et al., 2018). The validations of modeled depth-averaged current velocity and water level are shown in the middle panel and lower panel, separately.

friction coefficient and equals to 0.0026 according to Van Landeghem et al. (2009a); ν is kinematic viscosity coefficient; ρ is the density of seawater, and ρ_s is the density of sediment.

4. Results

4.1. Bedload convergence regions deduced by dunes

In the study area, we look into five areas which are all located at the dune asymmetry transition covering about 200–1000 m in the two sides of the inferred boundary lines (roughly outlined in Fig. 5). Regional sand transport directions deduced from dune migrations suggest that these five regions are likely bedload convergences. These bedload convergences hold either large symmetrical dunes on a negative seabed (lower than around seabed e.g. region A) or moderate dunes on thicker deposits (region E) (Fig. 5b). Here, dunes in the north side of region A migrate and have lee slopes dipping to the south, while dunes in the south side migrate and have lee slope inclining to the north (Fig. 6). It is different from regions C/region D, where sand dunes move to north/south in the west side and migrate to south/north in the east side

Table 1
Simulated and observed harmonic constants for four principal constituents (Simulation in the bracket where H is amplitude in cm and g is phase-lag referred to 120° E).

Site	Location	K1		O1		M2		S2	
		H	g	H	g	H	g	H	g
1	105.767°E/18.8°N	49 (47)	103 (109)	58 (60)	57 (54)	30 (34)	31 (32)	9 (10)	113 (120)
2	105.883°E/19.433°N	60 (67)	107 (113)	60 (54)	52 (56)	20 (24)	26 (23)	10 (11)	130 (128)
3	107.067°E/20.95°N	44 (52)	325 (336)	38 (40)	276 (280)	78 (74)	312 (310)	35 (30)	355 (359)
4	107.617°E/21.133°N	73 (69)	96 (106)	82 (79)	30 (38)	18 (15)	179 (187)	6 (5)	230 (231)
5	107.95°E/21.25°N	80 (83)	85 (94)	80 (84)	33 (32)	20 (18)	179 (187)	10 (12)	220 (222)
6	108.2°E/21.5°N	83 (70)	99 (100)	91 (88)	38 (42)	31 (25)	181 (192)	5 (6)	227 (225)
7	108.783°E/21.633°N	93 (92)	96 (106)	91 (98)	28 (30)	43 (42)	179 (161)	13 (10)	222 (199)
8	109.083°E/21.483°N	88 (75)	96 (101)	96 (93)	34 (33)	44 (37)	177 (183)	11 (9)	237 (242)
9	109.583°E/21.6°N	93 (92)	100 (115)	100 (95)	39 (36)	59 (55)	194 (214)	8 (10)	299 (277)
10	109.833°E/20.55°N	72 (77)	91 (103)	74 (84)	28 (32)	24 (25)	160 (167)	6 (12)	296 (292)
11	109.117°E/21.017°N	84 (72)	93 (103)	93 (90)	31 (34)	38 (32)	171 (182)	10 (8)	232 (235)
12	107.717°E/20.133°N	65 (69)	95 (101)	71 (65)	26 (27)	10 (12)	129 (122)	3 (3.7)	142 (140)
13	108.617°E/19.1°N	54 (51)	71 (81)	62 (55)	11 (12)	18 (19)	61 (73)	6 (6)	118 (111)

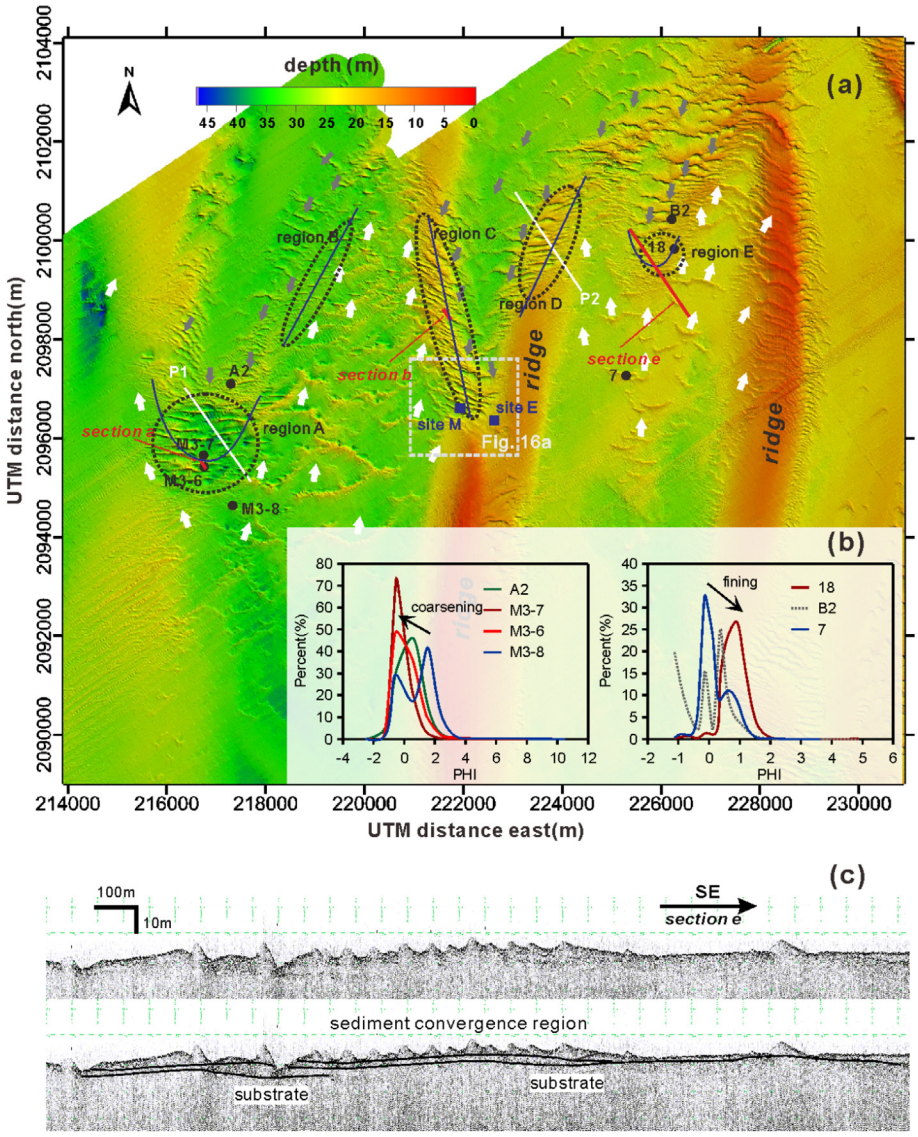

Fig. 5. Seabed topography of the study area and the five bedload convergence regions (A–E) of bedload convergence (a). White and gray arrows indicate the sense of dune asymmetry (point towards lee slopes). White line, red line, and dark dot separately represent the locations of the bathymetric profile, seismic profile, and sampling site. Blue lines are the inferred dune asymmetry transitional boundaries. Coordinates are in Universal Transverse Mercator projection (zone 49 N). (b) The coarsening and fining trends towards the middle of bedload convergence regions. (c) Seismic profiles of section *e* around region E. (For interpretation of the references to color in this figure legend, the reader is referred to the web version of this article.)

(Fig. 5). The asymmetrical sand dunes in the two sides of the convergences move together at speeds of several meters per year, and the migration speeds gradually decrease towards the highlighted regions (Fig. 7a). In the middle of the convergences, sand dunes present nearly symmetrical shapes and migrate at minimal speeds (lower than 2 m/y) although tidal current velocity is larger than 1 m/s (Xia et al., 2001; Ma et al., 2014). Moreover, there are apparent accretion on the crests and erosion in the troughs of dunes inside the convergences (region A)

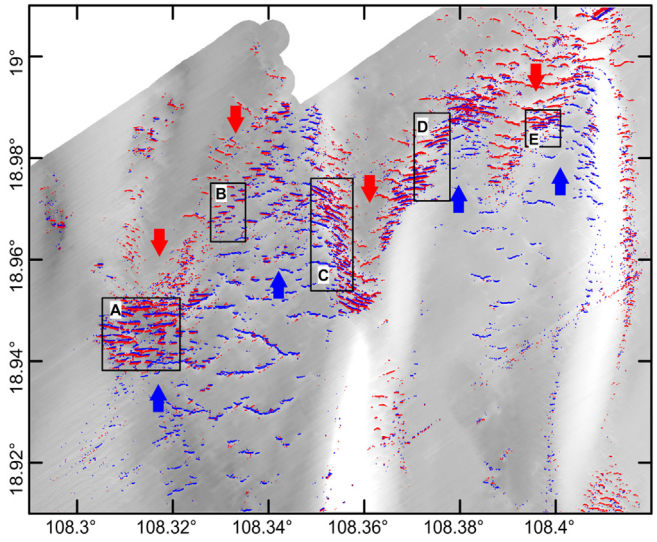

Fig. 6. Distribution of dune asymmetry, which is measured following the method of Ma et al. (2018). The blue line and the red line denote the steepest slopes of dunes inclining northward and southward, separately. Note the emergence of both red and blue lines in the regions A-E, which reflect their two steep sides and suggest nearly symmetrical shapes. The arrow also represents the inclination of dunes. (For interpretation of the references to color in this figure legend, the reader is referred to the web version of this article.)

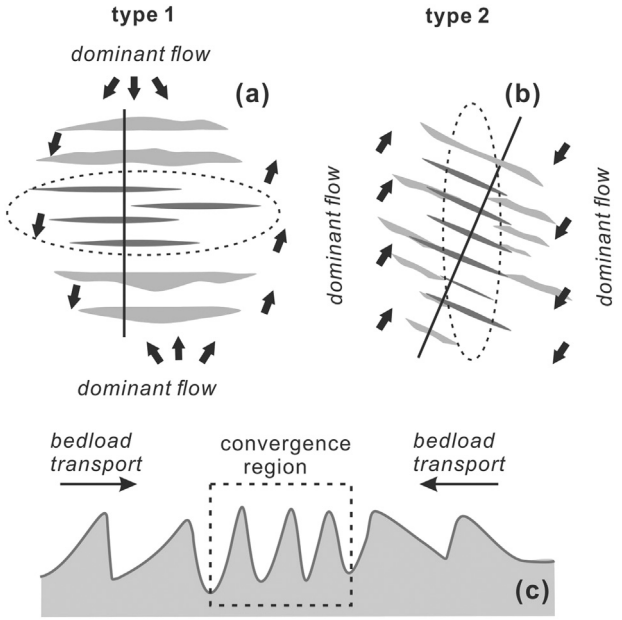

Fig. 8. Schematic diagram of the two kinds of dune asymmetry transition (a and b), both suggesting bidirectional sand transports from outside (c).

(Fig. 7b).

The five bedload convergence regions can be further classified into two types according to their distinct shapes and locations (Fig. 8). We suggest region A and region E as type 1 because they are both located in a relatively open area and sand dunes inside the regions extend to the west-east direction. The type 1 regions can be characterized by the asymmetry transition of dunes in their two sides. In contrast, type 2 region mostly consists of transitional parts of the dune individuals. The transitions mainly occur in the middle of the dune bodies in absence of separations. The type 2 regions are long and narrow and the dunes extend northwest-northeast (regions B, C, and D). It is different from the shearing zones where dunes can split into two parts as a result of the quick opposite migrations of their two ends (Caston, 1981; Franzetti et al., 2013; Schmitt et al., 2007). Besides, dune scale and assemblage are also varied in different regions even for the same type, which is probably associated with distinct local sediment supply conditions. For type 1, region A is mostly deeper than the around seafloor where relatively isolated and large dunes emerge. In contrast, region E has positive topography and the dunes are much smaller (Fig. 5). For type 2, dunes in region B are relatively small and discretely isolated whereas in other regions (C and D) dunes have larger scales and arrange closely.

4.2. Morphology of dunes around the bedload convergences

In the bedload convergence regions, most dunes arrange en-echelon and have trochoidal (Fig. 9) and nearly symmetrical or weak asymmetrical sections (about 67% of the total) (Fig. 10). The geometrical characters of ninety dunes were measured in the study area. The dunes have lengths of 20–180 m and heights of 1–15 m and exhibit a good correlation: $H = 0.0575\,L^{1.0836}$ ($R^2 = 0.834$) (Fig. 10). Even for a dune individual, this H-L relationship is still coherent in various sections along the crest (Fig. 11). This relation largely deviates from the Flemming's (1988) global mean relationship and is even steeper than the upper limit of Flemming's statistics ($H = 0.16\,L^{0.84}$) (Fig. 10). Dune height vs. water depth exhibits that more considerable water depth allows dunes to grow higher (Fig. 12). Some sand dunes even have heights exceeding a quarter of depths. As the water deepens to around 50 m, the dune height reaches up to nearly 15 m. The height-depth data mainly assemble in two separated zones. In Fig. 12, the light orange zone covers the H-D data of dunes from regions C, D, and E on the positive topography whereas the light blue zone contains the data from

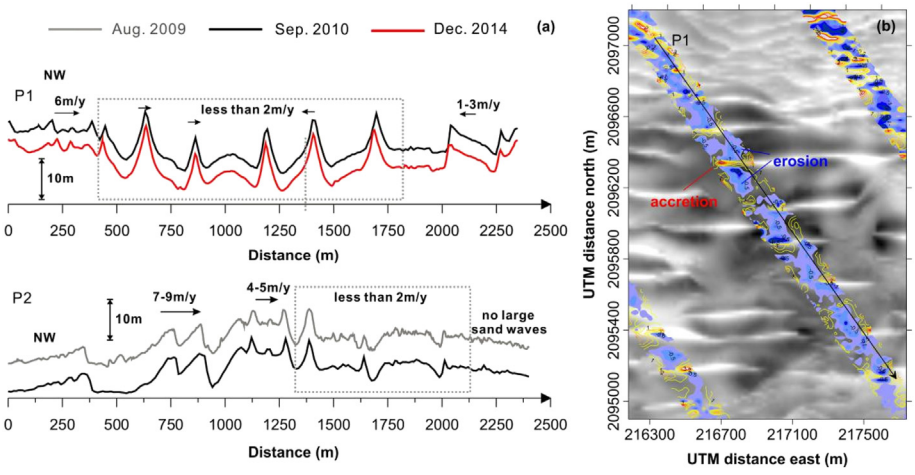

Fig. 7. (a) Comparisons of bathymetric profiles collected along the same lines marked in Fig. 5 at times indicated at the top. Note that the dunes moved convergently from the two sides and dunes around the dune asymmetry transitions have the slowest migrations. (b) Accretion (orange and red) on dune crests and erosion (blue) in dune troughs deduced by the bathymetric comparison between 2010 (band area) and 2014 (large map). White color denotes the shallowest and black color represents the deepest in the large map. Coordinates are in Universal Transverse Mercator projection (zone 49 N) as Fig. 5a and the location is also presented in Fig. 5. (For interpretation of the references to color in this figure legend, the reader is referred to the web version of this article.)

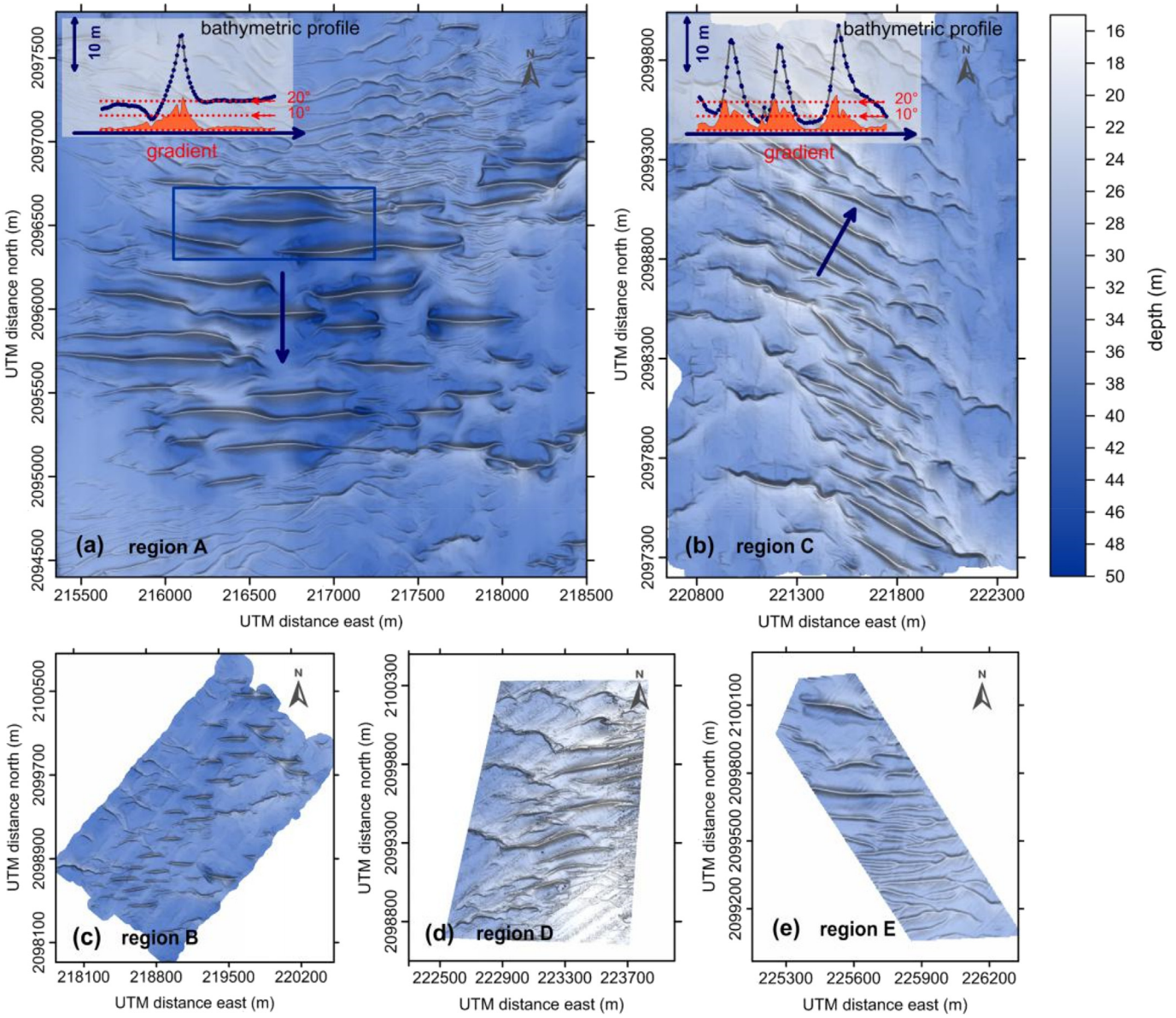

Fig. 9. Dunes with straight crests and steep sections in the five bedload convergence regions. Coordinates are in Universal Transverse Mercator projection (zone 49 N) as Fig. 5a. Blue lines with arrow in (a) and (b) locate the bathymetry (solid blue line with dots) and corresponding gradient (red) cross-sections shown. The red arrows point the gradient level of 20° and 10°, separately. (For interpretation of the references to color in this figure legend, the reader is referred to the web version of this article.)

the isolated dunes in regions A and B on the negative topography. Such distinct data assemblages may indicate two different growing trends of dunes under distinct sand supply conditions, in view of the limited sand supply on the negative topography (light blue zone) and sufficient supply on the positive topography (light orange zone).

4.3. Internal structures of dunes in the convergences

The study of internal structures provides a better understanding of dune behaviors, yet requires high-resolution seismic data. A hierarchy of bounding surfaces, which was established by Berné et al. (1988) in submarine dunes referring to the definitions in aeolian dunes (Brookfield, 1977), was often used on basis of their geometry and distribution. According to the terminology, first-order reflectors truncate underlying layers and mainly occur on the basement or the top. Second-order reflectors dip with a small angle and constitute the master-beddings. Third-order reflectors are steeper and interpreted as foresets.

Hence, seismic profiles of two typical sand dunes were interpreted following the above terminology. There are reflectors of all three orders inside the dunes (Fig. 13). The first-order reflectors are generally defined by the surface of dunes, the interface of reversing layers, and bases of dunes. Similar to the previous studies, second-order reflectors compose the central part of the host body. The third-order reflectors are also identified which are only limited on the lee side and nearly do not extend to the bottom. There is also a discernible interface in both dunes which exists between the two groups of reflections having opposite dipping directions (Fig. 13). The overlying layers are dipping to the north and the partly-preserved underlying layers are inclining to the south, indicating the reversal of past sand transport. Besides, the stratigraphy is not truncated on the crests but rather in the troughs, suggesting that dune troughs instead of dune crests are intensively scoured.

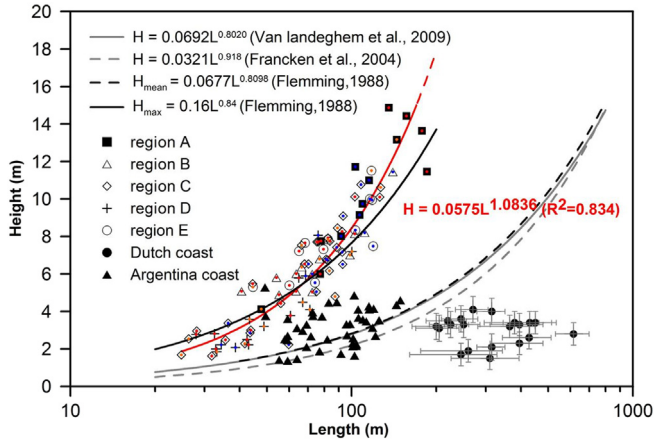

Fig. 10. Height versus length for 90 dunes measured in the regions, showing steeper shapes on average than that previous studies indicated. The red and orange dots separately represent dunes with asymmetrical parameters < 0.1 and 0.1–0.2, which represent nearly symmetrical and weak asymmetrical. Blue dots denote the parameters > 0.2. The nearly symmetrical or weak asymmetrical dunes account for about 67% of the total number. The black dots in the plot represent the data from dutch coast (Menninga, 2012) and the triangles are the data from Argentina coast (Salvatierra et al., 2015). (For interpretation of the references to color in this figure legend, the reader is referred to the web version of this article.)

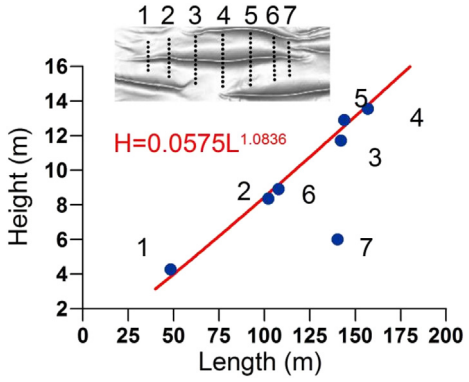

Fig. 11. Coherent H-L relation along the crest of a single dune. The location of the dune area is shown in Fig. 9 (blue frame). (For interpretation of the references to color in this figure legend, the reader is referred to the web version of this article.)

4.4. Regional and local tidal current characters

The modeled results show that tidal currents mainly flow to the north during flood and to the south during ebb, in keeping with the previous field observations (Xia et al., 2001). The tidal currents are energetic but display apparent spatial differences in both magnitude and direction (Fig. 14). During flood peak and ebb peak, tidal current speed can exceed 1.0 m/s in regions A, B, and E while the magnitude is relatively lower in regions C and D. The speed of currents in region D is smallest but still reaches up to 0.7 m/s. Residual currents direct oppositely in the two sides of the bedload convergences but flow almost parallel to the dune stretch directions inside the convergent regions (Fig. 14). It is accordant with the modeled net bedload transports (Fig. 15) and observed dune migrations in the study area (Ma et al., 2018). It indicates that residual currents and net bedload transports crossing convergences are weak, leading to the low dune migrations (inactive in the middle part) (Fig. 7). However, due to the low resolution of the grid (200 m), the model cannot reproduce detailed current regimes around the individual dunes in the study area which mostly have lengths smaller than 120 m.

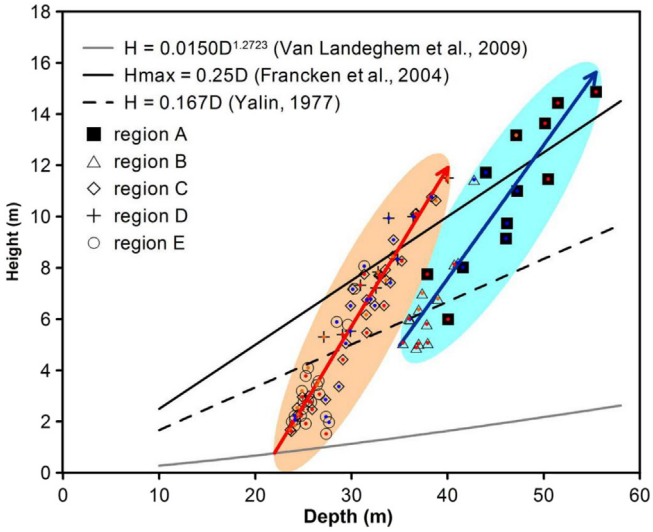

Fig. 12. Height-depth data of the dunes in the bedload convergences. Note that the data assemble in two main clusters and some heights exceed a quarter of depth. The color dots also represent asymmetrical parameters, as in Fig. 10. (For interpretation of the references to color in this figure legend, the reader is referred to the web version of this article.)

We here use the measured bottom currents to detect the detailed flow condition around the individual dunes in the dune asymmetry transitional area (Fig. 16). Measured results showed that the bottom currents were nearly reversing and asymmetrical in magnitude. Ebb currents were dominant at both sites and had the magnitude up to 75 cm/s; however, they flowed oppositely. On the seabed with no obstruction (site E), flood currents flowed to northward and ebb currents directed to southward (Fig. 16f) which were accordant with the simulated results. It was opposing to that in the dune trough (site M) where flood currents flowed southward and ebb currents were northward (Fig. 16c and d). Apparently, the reversed currents near the bottom are recorded over the lee side either in the flood period and in the ebb period. This unusual hydrodynamic regime, whereby the wakes from adjacent dunes overlap in subsequent half tidal cycles (Fig. 18), needs further investigation, preferably with shipboard ADCP surveys. However, this configuration suggests the dunes maybe squeezed (reduction in wavelength) closer together than normal due to convergent migration in this region. The convergent migration would also lead to higher H-L ration than are typically observed.

The sediments collected near regions A and E are coarse and mainly consist of sand and gravel. But the speeds of modern currents still exceed the threshold of sediment movement at most sites (Table 2) which means that the flows can move the sediment. Besides, the fining grain size trend towards region E (Fig. 5b) reflect the convergent transports because smaller grains in non-cohesive sediment can be started more easily. Such grain size trends are also in agreement with the modern regional flow distribution. It is opposing to region A where sediment becomes coarser from outside (A2 and M3-8) to inside (M3-7 and M3-6) of the region (Table 2, Fig. 5). The large proportion of coarse components inside region A may indicate that fine sediment can hardly move in, settling, or be kept inside the middle part, which is likely retarded by the large dunes on the boundary of the region. Such sediment distribution could be the results of the local flows influenced by the dunes rather than the regional flows.

5. Discussion

5.1. Morphological equilibrium of steep dunes in the convergences

Dune morphology is controlled by flows, basement, sediment nature

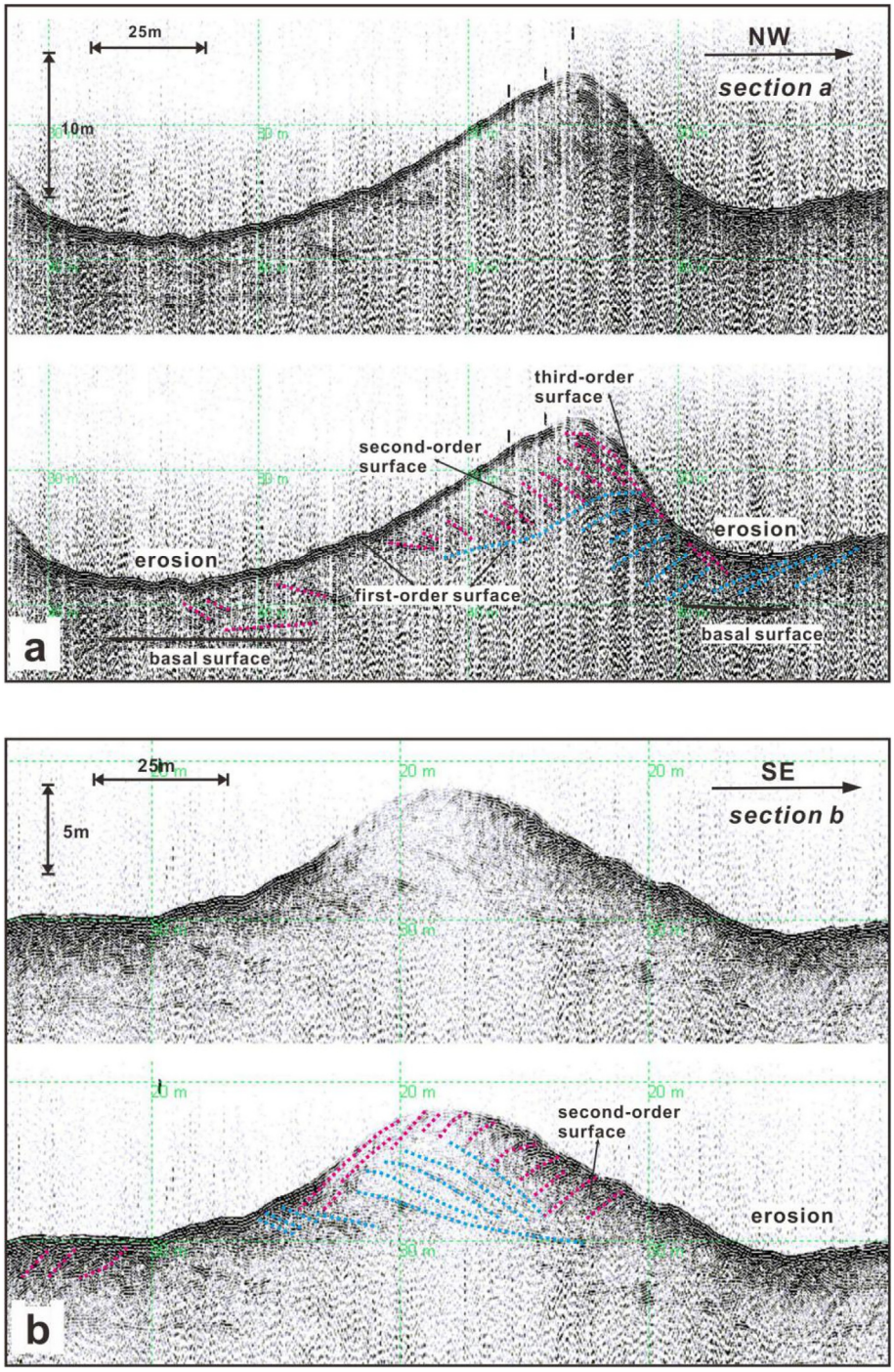

Fig. 13. Shallow seismic profiles and the interpreted internal structure of the two typical dunes. The locations of these two sections are denoted by short red lines in Fig. 5. (For interpretation of the references to color in this figure legend, the reader is referred to the web version of this article.)

and supply (Soulsby, 1997; Bartholdy et al., 2002; Van Landeghem et al., 2009b). Intrinsically, subaqueous mobile dunes are never in a static state as flow always fluctuates, which is similar to the aeolian dunes (Wasson and Hyde, 1983; El belrhiti and Douady, 2011; Melo et al., 2012). Thus the measured dune characteristics may imply a relatively balanced stage corresponding to ordinary hydrodynamics.

Basing on the worldwide data from different environments, Flemming (1988) proposed a relationship to represent the global mean H-L relation of dunes ($H = 0.0677\,L^{0.8098}$). It is usually assumed that dunes are in equilibrium with modern flows when H-L relation follows the global mean relationship of Flemming (1988). Many local cases have shown strikingly similar power law to further verify this correlation (Bartholdy et al., 2002; Wienberg and Hebbeln, 2005; Kubicki, 2008; Van Landeghem et al., 2009a, 2009b, 2012; Franzetti et al., 2013). However, the deviation of some individual dunes from the mean trend also needs to be considered. Van Landeghem et al. (2012) have suggested that the maximum steepness of the empirical function needs a revision because dunes in the Irish Sea are considerably steeper. Franzetti et al. (2013) provided another case of steep dunes on a deep shelf. These two cases presented different correlations between height and length, which were attributed to complex build-ups related to multi-parameters. Here, the steepness of H-L relation is somewhat larger than Flemming's maximum trend, supporting the suggestion of Van Landeghem et al. (2012). The H-L relationship is coherent in

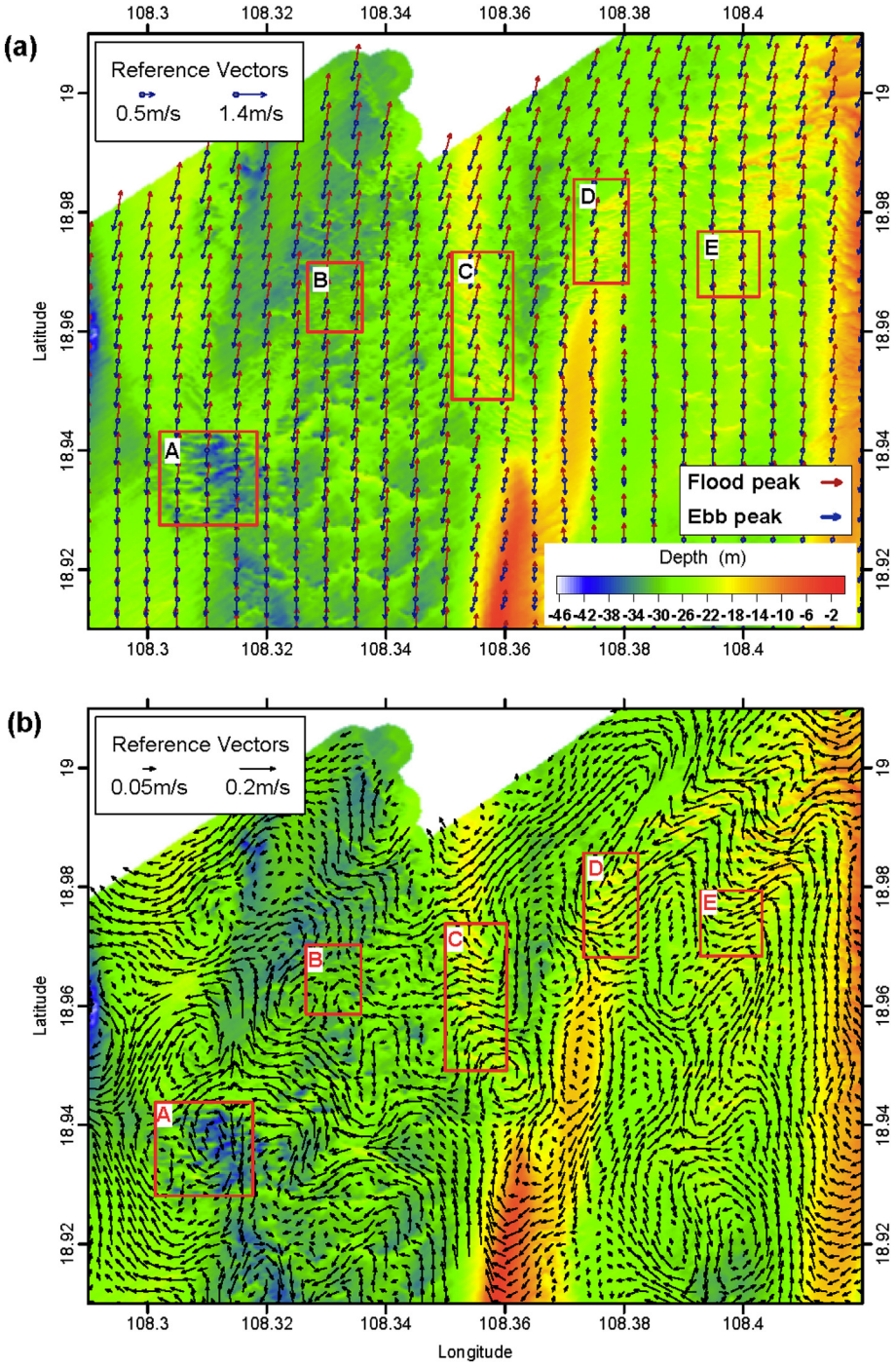

Fig. 14. Simulated depth-averaged tidal currents at flood peak and ebb peak (a) and the residual currents (b) in the study area.

different dunes even though they develop in various regions. We thus recommend that the H-L correlation here is universal for the dunes near dune asymmetry transition where they receive bi-directional sand supply. Previous model studies have successfully shown that the heights of tidal dunes are associated with water depth (Besio et al., 2006; Blondeaux and Vittori, 2011; Van Santen et al., 2011). Due to the constriction of flow and water thickness, heights of sand waves are inferred to be smaller than a quarter of water depths in river environments (Francken et al., 2004). However, in the study area, some dune heights have exceeded Francken's upper limit, and the maximum height even reaches up to nearly 15 m at a depth of 50 m. Such large heights could be benefited from the bi-directional sand supply, preserved sand body, and erosion in the troughs (Fig. 13).

5.2. How dunes maintain the steep and straight shapes under strong reversing currents?

In the study area, the modern currents can modify the dunes as they can move the sediment. But interestingly, the steepness and heights of dunes have not been constrained. Storms have not constrained the dune steepness either, although they can result in strong orbital velocity on crests and cause erosion. If frequent erosion happens on the crests, the sediment eroded from the crests will easily deposit in the neighboring troughs. However, we did not find legible truncations in the subsurface layers on the crests; instead, erosion distinctly occurs in the troughs. Crossing beddings in dunes were often regarded as the results of storm-induced currents (Ma et al., 2013). However, there seems only one

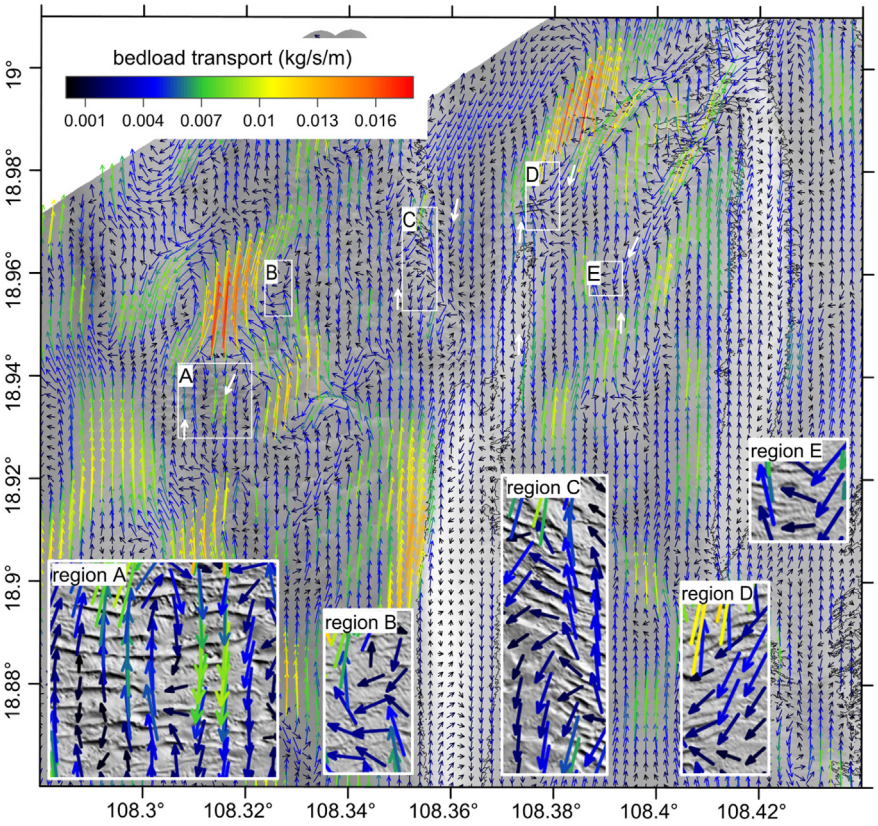

Fig. 15. The calculated net bedload transport during a spring-neap tidal cycle in the study area (modified from Ma et al., 2018). The white arrows denote the inclination of dunes. The regions A-E are enlarged in the subfigures which exhibit the weak net bedload transports parallel to the dune extending directions.

discernible layer reversal in the dunes (Fig. 13) and the layer inclination reverses permanently instead of frequent reversing. It means that storms cannot determine the shapes of dunes in the study area. But nonetheless, we believe that storms can produce large amounts of suspension and largely enhance local sediment transport (both as bedload and suspension) (Schmitt and Mitchell, 2014), in a short-term period. The long-term trend of sediment transport cannot be changed by short-term events (Ma et al., 2013). Therefore, the shapes of dunes could be largely dominated by the long-term tidal currents. The storm-induced suspension occurring around the dunes and its relation to dune figuration need to be further studied, both on modeling and field observation.

The opposite asymmetry and migration of dunes and trends of grain size reflect regionally convergent net sand transports from the two sides of the dune asymmetry transitional areas. Even inside the regions, the local pile-ups (Fig. 5b) also occur on the dune individuals from the two flanks (or troughs in the two sides). Such bi-directional sand supply (both regional and local) provides the primary source for the vertical construction of dunes. Hence, the induced accretion and some underlying topography both contribute to the large dune heights and scale. The steep shape is also benefited from the down-cutting or erosion in the troughs and in the lower part of lee flanks (Figs. 7b and 13). The down-cutting enhances the vertical heights by deepening the troughs and limit the enlargement of dune lengths. The erosion in the lower lee flank or troughs is most likely associated with the reversed flow and turbulence related to flow separations (Figs. 15 and 16). Such reversed flows can also produce oblique sediment transports to the lee slope and drive sediment transport in troughs in the along-crest direction, helping mould the dune forms (Walker, 1999; Walker and Nickling, 2002, 2003). These processes in the interdune zones can interpret the occurrence of sand ripples in the trough and on the two flanks (Fig. 15b).

The straight or very slightly curved crests of dunes can also be attributed to the bi-directional/bimodal flow regimes. In the study area, most dunes have orientations almost normal to the reversing tidal currents which have spread angles much larger than 90°. According to Rubin and Hunter (1987), bedform alignment is controlled by the angle between the flood and ebb currents and the proportion of sand transport in those two directions. Dune crests should be normal to the maximum gross transport. For bimodal flow regimes with flow direction differences of 90° to 180° and similar current speeds during flood and ebb, weakly asymmetric transport is produced. Such flow regimes lead to nearly symmetrical sections of dunes and also increase along-crest transport proportion to elongate crests and make them straighter (Rubin, 2012). These effects on crests have been identified on intertidal dunes under reversing flows (Lee et al., 2006) and on aeolian bedforms like linear dunes (Parteli et al., 2009; Reffet et al., 2010) or wave ripples (Harms, 1969). We here provide cases for the bi-directional mode in the shallow shelves. Parteli et al. (2009) suggested that variety in heights and lasting time of flows in the two directions could trigger wavy crests. Here, the meandering crests of such dunes are very weak which may indicate the similar lasting time of the reversing currents over the convergences.

5.3. Flow separation on the two flanks of dunes in the convergences

As discussed above, our results reveal that flow separation could have substantial impacts on the shape development of dunes. Flow separation is known to depend on roughness and Reynolds number and is related to dune lee slope (Kwoll et al., 2016). Kadota and Nezu (1999) demonstrated that the DSL (Dimensionless Separation Length) decreases with increasing *Re* (Reynolds number) in cases with solitary bedforms and $Re < 20{,}000$ and reach a constant value of about 6.5 at $Re > 20{,}000$. The DSL is about 4.5 at any Reynolds number in cases with multiple bedforms (Fig. 17a). The study of Engel (1981) showed

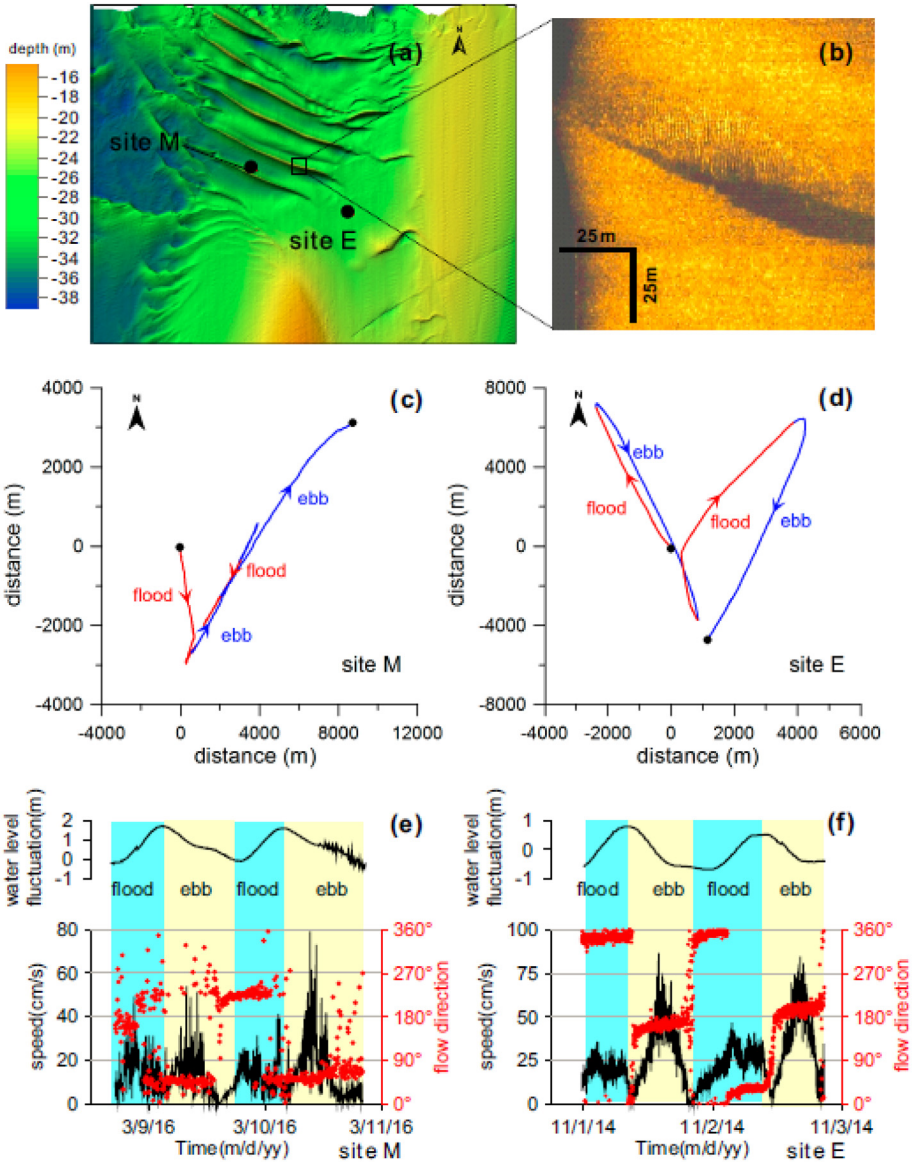

Fig. 16. Bottom current measurements at two sites around the dunes. (a) The location of the two sites. (b) The sonar image of the dunes with ripples arranging obliquely or normal to the crest of the host on the dune flank. (c and d) The progressive vector plots of the bottom currents, indicating nearly opposite flow directions inside and outside the dune troughs during the same tidal period. (e and f) The time-series of observed bottom currents at site M in March 2016 and at site E in November 2014.

that the DSL was about 4.5 when the dune steepness (H/L) was larger than 0.07; otherwise the DSL increased with the decrease of dune steepness and the increase of grain size (Fig. 17b). Previous studies also showed that a flow separation zone emerged on the steep lee side of dunes and the separated shear layer re-attaches at approximately 4–6 times of the dune-height length downstream the crest (cf. reviews of Best, 2005). Wilbers (2004) defined the zero-velocity-line inside the flow separation region which has an approximate angle of 10° from the brink point towards flow reattachment defining the upper boundary of reversed flow area. The flow moves reversely (upstream) below this

Table 2
Grain size of sediments recovered from the grab sites located in Fig. 5.

Site	Median size (μm)	Grain size distribution				Textural group	Depth-averaged threshold velocity (cm/s)
		%Gravel	%Sand	%Silt	%Clay		
M3-7	1506	33.99	65.49	0.44	0.08	Gravelly sand	57.7
M3-6	984	26.93	71.59	1.20	0.28	Gravelly sand	43.4
M3-8	473	10.60	87.97	1.15	0.28	Gravelly sand	29.4
A2	807	2.81	96.55	0.62	0.02	Sand	38.4
7	1019	19.80	80.17	0.02	0	Gravelly sand	44.4
18	564	0.21	99.7	0.09	0	Sand	31.8
B2	959	0.3	99.7	0	0	Sand	42.7

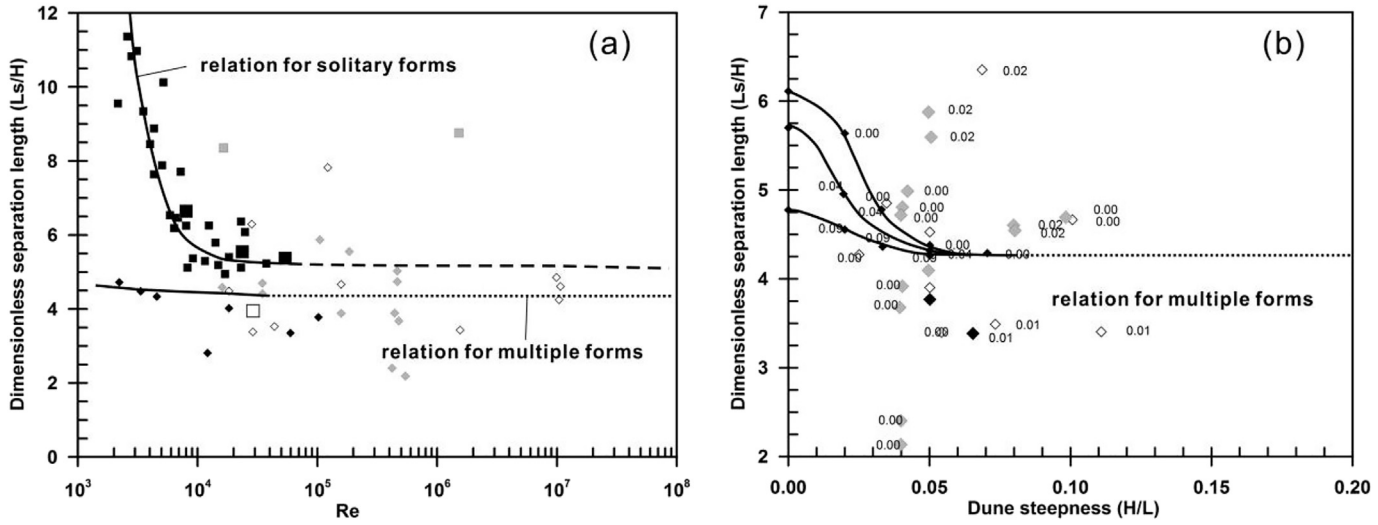

Fig. 17. Relations between dimensionless separation length (Ls/H) and Reynold's number and dune steepness (H/L) (modified from Wilbers (2004)). In (a), big squares are the data points of Wilbers (2004), while the other points are from the data of Kadota and Nezu (1999). In (b), big diamonds are also the data points of Wilbers (2004), while the other ones are the data of Engel (1981), and the numbers beside each point show the dimensionless grain size (D_{50}/H).

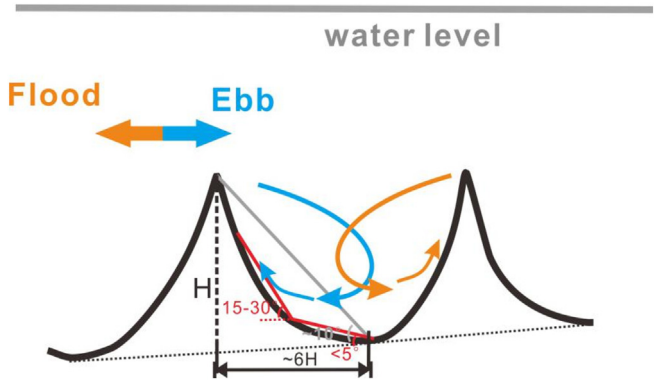

Fig. 18. Diagram of interpreted flow reversals on the two flanks of large dunes during a tidal cycle under nearly symmetrical reversing currents. Note the gradient variations across the dune flanks.

zero velocity line and moves forward to reattach the stoss side of the downstream dune. As most dunes have weak asymmetry, we simplify the dune section to be a symmetrical triangle to calculate the slope angles of flanks. We find that the length of stoss/lee side of dunes are both about six times of the height (H/L~1/12) and the flank slope is approximate 10° in both sides of dunes (Fig. 18). This matches well with the flow separation range predicted according to Wilbers (2004) and Best (2005). It indicates that the trochoidal shapes of dunes are closely related to the flow separations and flow reversals over the lee flanks of dunes. Herein, the flow reversals have been captured near bottom in both flanks of the steep dunes (Figs. 16 and 18). The observation shows overlapped flow reversals during flood and ebb, which could be ascribed to the close distance of the adjacent steep dunes and the strong flood/ebb tidal currents leading to vortices in the most part of the interdune area. Certainly, simulations and field observations such as shipboard ADCP, are still required and encouraged to look into more details of such unique flow condition between the adjacent steep dunes.

The flow separations occur permanently or occasionally? Some researchers reported that permanent flow separation occurred on the lee side steeper than 10° (Wilbers, 2004; Paarlberg et al., 2009), whereas the critical lee slope was suggested to be 15° through negative step experiments (Ruck and Makiola, 1993). Kwoll et al. (2016) found through simulation that flow reversals downstream the dunes were only absent when the lee slope ≪ 10°. Here, the slope angle of the flank is not uniform but gradually increases from the bottom of flanks to the crest of dunes. The upper part of some flanks has a slope much larger than 10° (some almost approach 30°), while the lower part of flanks only has a slope angle smaller than 5°. It leads to the conclusion that flow separation is intermittent in both flanks for most dunes and permanent for some high individuals, which long-term maintains the steep shapes of dunes.

5.4. Scale determination of the steep dunes under nearly symmetrical reversing currents

In the study area, sand dunes in the bedload convergence regions are much steeper than other areas. The H-L relation keeps coherent and is independent of dune scale and distribution, grain size, internal structures, and sediment supply condition. Hence, the geometry of such dunes (H-L relation, straightness) in different areas should be attributed to similar flow regimes. We here argue that the dunes are in equilibrium with the modern tidal currents which carve out and maintain the steep shapes of dunes. Herein, we assume that the nearly symmetrical regional currents have roughly sustained for decades or several hundreds of years which allow the evolution of huge dunes under a relatively stable tide environment. This is different from the similar sand dunes found in the Irish Sea which were inferred to be relics (Van Landeghem et al., 2009a).

Distinct to the geometry, there are two directions for the scale determination of dunes which mostly depend on different sand supply conditions (Figs. 12 and 19). Positive topography higher than the around seabed (regions C, D, and E) has indicated there was a large amount of source supporting the dune growth (Fig. 5c and Fig. 9). Dunes can grow to a large scale with the suggested H-L relation (Fig. 12) under sufficient sand supply. When dune height reaches up to a large value, the external sand supply would be somewhat retarded by the dunes (Fig. 5) and erosion occurs in the troughs in the internal part of the regions (region A) (Fig. 13). As in region A, down-cutting occurs in the trough and leads the dunes to be more self-reliant by separating the neighboring individuals (Fig. 9a). The straight transverse dunes also break more easily and split into separated ones (Fig. 9a). Because of the lack of sand supply, the broken dunes cannot recover and the newborn smaller individuals mostly develop into fusiform shapes to adapt to the nearly symmetrical reversing currents and maintain the H-L relation along the crests (Fig. 9a and c, Fig. 19). On the other hand, when the external sand supply is limited such as region B, the dunes can hardly

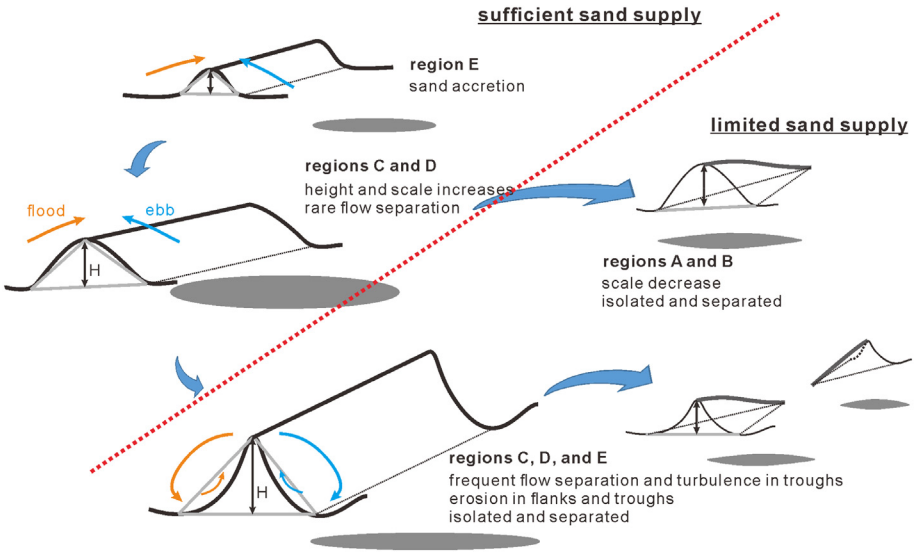

Fig. 19. Scale determination of steep dunes under different sand supply conditions under modern nearly symmetrical or weak asymmetrical currents. The orange and light blue arrows represent flows and related sediment transport during flood or ebb. (For interpretation of the references to color in this figure legend, the reader is referred to the web version of this article.)

grow to a large scale at the early stage and preferentially keep the H-L relation in their small scales and become more self-contained and susiform (Figs. 9c and 12). This interprets the occurrence of the small fusiform dunes and erosion around them inside region A and region B. Therefore, in the regions under bi-directional flows, sediment supply condition may determine the scales of dunes, while the local flow regimes dominate the steep shapes.

6. Conclusion

This study detailedly documents the morphology and maintenance of the steep and nearly symmetrical dunes around bedload convergences in Beibu Gulf, northwest South China Sea. The results show that the dunes have analog shapes with steep sections and relatively straight crests. Length and height of the dunes display a general good correlation relation: $H = 0.0575\,L^{1.0836}$ ($R^2 = 0.834$), which is steeper than other relationships. Some dunes have extraordinary heights, which can be ascribed to combined influences of bidirectional sand accretion on the crests, the preserved sand body, and erosion in the troughs. The H-L relation of the dunes is independent of dune scale, dune internal structure, and sand grain size, and is suggested to be the universal relationship for the dunes under bi-directional sand supply. Herein, the straight crests, the steep shapes, and the uniform H-L relation of dunes all adapt to the prevailing tidal currents. Nearly symmetrical or weak asymmetrical tidal currents result in the bedload convergences and the accretions occur in the convergences. In the convergences, local flows are largely influenced by the dunes leading to the modification of flow structures over the lee side. Flow separations and related energetic flow reversals are caused on either flanks of dunes, leading to erosion in troughs and flanks. The large dunes, in turn, obstruct the cross-crest sand transport from external and affect the transport patterns inside the regions. To sum up, sand supply condition mainly determine the scales of dunes, while the flow regimes determined the steep and straight shapes.

The study is focused on the morphology, build-up processes, and maintenance of dunes around the bedload convergences mainly basing on field surveys. We hope it can help widen our understanding of dune morphology and dune behavior on shallow shelves. It is also expected to contribute to the further development of models on the formation and evolution of such subaqueous dunes. Future observation and experiment of flow structures over the flanks in such two-side steep dunes are still required. Models are also expected to address their detailed growth and evolution processes of such steep dunes.

Acknowledgment

We thank Zhendong Luan, Changan Chen of Institute of Oceanology, Chinese Academy of Sciences for their efforts in collecting and processing the multibeam bathymetric data. We also thank the crews on board the R/V Kexue-III for collecting the field data. This study was funded by the National Natural Science Foundation of China (41876035, 41406061). We appreciate Editor Edward Anthony, Dr. N.C. Mitchell, and the other anonymous reviewer for their constructive comments and suggestions which largely improve our manuscript.

Appendix A. Supplementary data

Supplementary data to this article can be found online at https://doi.org/10.1016/j.margeo.2019.03.006.

References

Allen, J.R.L., 1980. Sand waves: a model of origin and internal structure. Sediment. Geol. 26, 281–328.
Anthony, D., Leth, J.O., 2002. Large-scale bedforms, sediment distribution and sand mobility in the eastern North Sea off the Danish west coast. Mar. Geol. 182, 247–263. https://doi.org/10.1016/S0025-3227(01)00245-6.
Ashley, G.M., 1990. Classification of large-scale subaqueous bedforms; a new look at an old problem. J. Sediment. Res. 1, 160–172. https://doi.org/10.2110/jsr.60.160.
Barnard, P.L., Hanes, D.M., Rubin, D.M., Kvitek, R.G., 2006. Giant sediment waves at the mouth of San Francisco Bay. EOS Trans. Am. Geophys. Union 87, 285.
Bartholdy, J., Bartholomae, A., Flemming, B.W., 2002. Grain-size control of large compound flow-transverse bedforms in a tidal inlet of the Danish Wadden Sea. Mar. Geol. 188, 391–413. https://doi.org/10.1016/S0025-3227(02)00419-X.
Berné, S., Auffret, J.P., Walker, P., 1988. Internal structure of subtidal sandwaves revealed by high-resolution seismic reflection. Sedimentology 35, 5–20. https://doi.org/10.1111/j.1365-3091.1988.tb00902.x.
Berné, S., Castaing, P., Le Drezen, E., Lericolais, G., 1993. Morphology, Internal Structure, and Reversal of Asymmetry of Large subtidal Dunes in the Entrance to Gironde Estuary (France). J. Sediment. Res. 63, 780–793. https://doi.org/10.1306/D4267C03-2B26-11D7-8648000102C1865D.
Besio, G., Blondeaux, P., Frisina, P., 2003. A note on tidally generated sand waves. J. Fluid Mech. 485, 171–190. https://doi.org/10.1017/S0022112003004415.
Besio, G., Blondeaux, P., Brocchini, M., Vittori, G., 2004. On the modeling of sand wave migration. J. Geophys. Res. 109, C04018. https://doi.org/10.1029/2002JC001622.
Besio, G., Blondeaux, P., Vittori, G., 2006. On the formation of sand waves and sand banks. J. Fluid Mech. 557, 1–27. https://doi.org/10.1017/S0022112006009256.
Besio, G., Blondeaux, P., Brocchini, M., Hulscher, S., Idier, D., Knaapen, M.A.F., Németh, A.A., Roos, P.C., Vittori, G., 2008. The morphodynamics of tidal sand waves: a model overview. Coast. Eng. 55, 657–670. https://doi.org/10.1016/j.coastaleng.2007.11.004.
Best, J., 2005. The fluid dynamics of river dunes: a review and some future research directions. J. Geophys. Res. 110, F04S02. https://doi.org/10.1029/2004JF000218.
Blondeaux, P., Vittori, G., 2011. The formation of tidal sand waves: fully three-dimensional versus shallow water approaches. Cont. Shelf Res. 31, 990–996. https://doi.org/10.1016/j.csr.2011.03.005.

Brookfield, M.E., 1977. The origin of bounding surfaces in ancient eolian sandstones. Sedimentology 24, 303–332. https://doi.org/10.1111/j.1365-3091.1977.tb00126.x.
Cao, L.H., Xu, J.S., Li, G.X., Shi, J.H., 2006. High-resolution morphological characteristics of sand waves off the west Hainan Island. Mar. Geol. Quat. Geol. 26, 15–22 (in Chinese).
Caston, G.F., 1981. Potential gain and loss of sand by some sand banks in the Southern Bight of the North Sea. Mar. Geol. 41, 239–250. https://doi.org/10.1016/0025-3227(81)90083-9.
Dalrymple, R.W., 1978. Bedforms and their hydraulic stability relationships in a tidal environment, Bay of Fundy, Canada. Nature 275, 100–104. https://doi.org/10.1038/275100a0.
Dalrymple, R.W., Rhodes, R.N., 1995. Chapter 13 estuarine dunes and bars. In: Developments in Sedimentology. Elsevier, pp. 359–422.
Duffy, G.P., 2012. Patterns of morphometric parameters in a large bedform field: development and application of a tool for automated bedform morphometry. Irish J. Earth Sci. 30, 31–39. https://doi.org/10.3318/IJES.2012.30.31.
El belrhiti, H., Douady, S., 2011. Equilibrium versus disequilibrium of barchan dunes. Geomorphology 125, 558–568. https://doi.org/10.1016/j.geomorph.2010.10.025.
Engel, P., 1981. Length of flow separation over dunes. J. Hydraul. Div. 107, 1133–1143.
Ernstsen, V.B., Noormets, R., Winter, C., Hebbeln, D., Bartholomä, A., Flemming, B.W., Bartholdy, J., 2006. Quantification of dune dynamics during a tidal cycle in an inlet channel of the Danish Wadden Sea. Geo-Mar. Lett. 26, 151–163. https://doi.org/10.1007/s00367-006-0026-2.
Ferret, Y., Le Bot, S., Tessier, B., Garlan, T., Lafite, R., 2010. Migration and internal architecture of marine dunes in the eastern English Channel over 14 and 56 year intervals: the influence of tides and decennial storms. Earth Surf. Process. Landf. 35, 1480–1493. https://doi.org/10.1002/esp.2051.
Flemming, B.W., 1988. Zur Klassifikation subaquatischer, strömungstransversaler Transportkörper. Bochum. Geol. Geotechn. Arb. 29, 93–97.
Francken, F., Wartel, S., Parker, R., Taverniers, E., 2004. Factors influencing subaqueous dunes in the Scheldt Estuary. Geo-Mar. Lett. 24, 14–21. https://doi.org/10.1007/s00367-003-0154-x.
Franzetti, M., Le Roy, P., Delacourt, C., Garlan, T., Cancouët, R., Sukhovich, A., Deschamps, A., 2013. Giant dune morphologies and dynamics in a deep continental shelf environment: example of the Banc du Four (Western Brittany, France). Mar. Geol. 346, 17–30. https://doi.org/10.1016/j.margeo.2013.07.014.
Gerkema, T., 2000. A linear stability analysis of tidally generated sand waves. J. Fluid Mech. 417, 303–322. https://doi.org/10.1017/S0022112000001105.
Harms, J.C., 1969. Hydraulic significance of some sand ripples. Geol. Soc. Am. Bull. 80, 363–396. https://doi.org/10.1130/0016-7606(1969)80[363:HSOSSR]2.0.CO;2.
Hulscher, S.J., 1996. Tidal-induced large-scale regular bed form patterns in a three-dimensional shallow water model. J. Geophys. Res. 101, 20727–20744.
Hulscher, S.J., de Swart, H.E., de Vriend, H.J., 1993. The generation of offshore tidal sand banks and sand waves. Cont. Shelf Res. 13, 1183–1204. https://doi.org/10.1016/0278-4343(93)90048-3.
Kadota, A., Nezu, I., 1999. Three-dimensional structure of space-time correlation on coherent vortices generated behind dune crest. J. Hydraul. Res. 37, 59–80. https://doi.org/10.1080/00221689909498532.
Knaapen, M.A.F., 2005. Sandwave migration predictor based on shape information. J. Geophys. Res. 110, F04S11. https://doi.org/10.1029/2004JF000195.
Komarova, N.L., Hulscher, S.J., 2000. Linear instability mechanisms for sand wave formation. J. Fluid Mech. 413, 219–246. https://doi.org/10.1017/S0022112000008429.
Kubicki, A., 2008. Large and very large subaqueous dunes on the continental shelf off southern Vietnam, South China Sea. Geo-Mar. Lett. 28, 229–238. https://doi.org/10.1007/s00367-008-0103-9.
Kwoll, E., Venditti, J.G., Bradley, R.W., Winter, C., 2016. Flow structure and resistance over subaqueous high- and low-angle dunes. J. Geophys. Res. Earth Surf. 121, 545–564. https://doi.org/10.1002/2015JF003637.
Le Bot, S., Trentesaux, A., 2004. Types of internal structure and external morphology of submarine dunes under the influence of tide- and wind-driven processes (Dover Strait, northern France). Mar. Geol. 211, 143–168. https://doi.org/10.1016/j.margeo.2004.07.002.
Lee, H.J., Jo, H.R., Yong, S.C., 2006. Dune migration on macrotidal flats under symmetrical tidal flows: Garolim Bay, Korea. J. Sediment. Res. 76, 284–291. https://doi.org/10.2110/jsr.2006.027.
Lobo, F.J., Hernández-Molina, F.J., Somoza, L., Rodero, J., Maldonado, A., Barnolas, A., 2000. Patterns of bottom current flow deduced from dune asymmetries over the Gulf of Cadiz shelf (southwest Spain). Mar. Geol. 164, 91–117. https://doi.org/10.1016/S0025-3227(99)00132-2.
Lobo, F.J., Maldonado, A., Noormets, R., 2010. Large-scale sediment bodies and superimposed bedforms on the continental shelf close to the Strait of Gibraltar: interplay of complex oceanographic conditions and physiographic constraints. Earth Surf. Process. Landf. 35, 663–679. https://doi.org/10.1002/esp.1962.
Ma, X., Yan, J., Fan, F., Yao, P., 2013. Response of bedload transport, submarine topography, and dune internal structures to typhoon processes off Dongfang coast in the Beibu Gulf. Acta Oceanol. Sin. 32, 27–40. https://doi.org/10.1007/s13131-013-0296-2.
Ma, X., Yan, J., Fan, F., 2014. Morphology of submarine barchans and sediment transport in barchans fields off the Dongfang coast in Beibu Gulf. Geomorphology 213, 213–224. https://doi.org/10.1016/j.geomorph.2014.01.010.
Ma, X., Li, J., Yan, J., 2018. Tide-induced bedload transport pathways in a multiple-sand-ridge system offshore of Hainan Island in the Beibu Gulf, northwest South China Sea. Earth Surf. Process. Landf. 43, 2738–2753. https://doi.org/10.1002/esp.4428.
McManus, J., 1988. Grain size determination and interpretation. In: Tucker, M. (Ed.), Techniques in Sedimentology. Blackwell, Oxford, pp. 63–85.
Melo, H.P.M., Parteli, E.J.R., Andrade Jr., J.S., Herrmann, H.J., 2012. Linear stability analysis of transverse dunes. Physica A 391, 4606–4614. https://doi.org/10.1016/j.physa.2012.05.042.
Menninga, P.J., 2012. Analysis of Variations in Characteristics of Sand Waves Observed in the Dutch Coastal Zone: A Field and Model Study. (Master's thesis).
Mosher, D.C., Thomson, R.E., 2000. Massive submarine sand dunes in the eastern Juan de Fuca Strait, British Columbia. In: Trentesaux, A., Garlan, T. (Eds.), Marine Sandwave Dynamics, Proceedings, International Workshop. University of Lille 1, France, pp. 131–142.
Németh, A.A., Hulscher, S.J.M.H., de Vriend, H.J., 2002. Modelling sand wave migration in shallow shelf seas. Cont. Shelf Res. 22, 2795–2806. https://doi.org/10.1016/S0278-4343(02)00127-9.
Németh, A.A., Hulscher, S.J.M.H., Van Damme, R.M.J., 2007. Modelling offshore sand wave evolution. Cont. Shelf Res. 27, 713–728. https://doi.org/10.1016/j.csr.2006.11.010.
Paarlberg, A.J., Dohmen-Janssen, C.M., Hulscher, S.J.M.H., Termes, P., 2009. Modeling river dune evolution using a parameterization of flow separation. J. Geophys. Res. 114, F01014. https://doi.org/10.1029/2007JF000910.
Parteli, E.J.R., Durán, O., Tsoar, H., Schwämmle, V., Herrmann, H.J., 2009. Dune formation under bimodal winds. Proc. Natl. Acad. Sci. U. S. A. 106, 22085–22089. https://doi.org/10.1073/pnas.0808646106.
Reffet, E., Courrech du Pont, S., Hersen, P., Douady, S., 2010. Formation and stability of transverse and longitudinal dunes. Geology 38, 491–494. https://doi.org/10.1130/G30894.1.
Rubin, D.M., 2012. A unifying model for planform straightness of ripples and dunes in air and water. Earth-Sci. Rev. 113, 176–185. https://doi.org/10.1016/j.earscirev.2012.03.010.
Rubin, D.M., Hunter, R.E., 1987. Bedform alignment in directionally varying flow. Science 237, 276–278.
Ruck, B., Makiola, B., 1993. Flow separation over the inclined step. In: Gersten, K. (Ed.), Physics of Separated Flows—Numerical, Experimental and Theoretical Aspects, Notes on Numer. Fluid Mech. 40. Springer Vieweg, Wiesbaden, pp. 47–55.
Salvatierra, M.M., Salvador, A., Silvia, S.G., 2015. Morphology and dynamics of large subtidal dunes in Bahia Blanca estuary, Argentina. Geomorphology 246, 168–177.
Schmitt, T., Mitchell, N.C., 2014. Dune-associated sand fluxes at the nearshore termination of a banner sand bank (Helwick Sands, Bristol Channel). Cont. Shelf Res. 76, 64–74.
Schmitt, T., Mitchell, N.C., Ramsay, T.S., 2007. Use of swath bathymetry in the investigation of sand dune geometry and migration around a near shore 'banner' tidal sandbank. Geol. Soc. Lond., Spec. Publ. 274, 53–64.
Schmitt, T., Mitchell, N.C., Ramsay, T.S., 2008. Characterizing uncertainties for quantifying bathymetry change between time-separated multibeam echo-sounder surveys. Cont. Shelf Res. 28, 1166–1176.
Soulsby, R., 1997. Dynamics of marine sands. In: A Manual for Practical Applications. Thomas Telford Services Ltd., London.
Soulsby, R.L., Whitehouse, R.J.S., 1997. Threshold of sediment motion in coastal environments. In: Pacific Coasts and Ports' 97: Proceedings of the 13th Australasian Coastal and Ocean Engineering Conference and the 6th Australasian Port and Harbour Conference. volume 1. Centre for Advanced Engineering, University of Canterbury, pp. 145.
Todd, B.J., Shaw, J., Li, M.Z., Kostylev, V.E., Wu, Y., 2014. Distribution of subtidal sedimentary bedforms in a macrotidal setting: the Bay of Fundy, Atlantic Canada. Cont. Shelf Res. 83, 64–85. https://doi.org/10.1016/j.csr.2013.11.017.
Van der Veen, H.H., Hulscher, S.J.M.H., Knaapen, M.A.F., 2006. Grain size dependency in the occurrence of sand waves. Ocean Dyn. 56, 228–234. https://doi.org/10.1007/s10236-005-0049-7.
Van Dijk, T.A., Kleinhans, M.G., 2005. Processes controlling the dynamics of compound sand waves in the North Sea, Netherlands. J. Geophys. Res. Earth Surf. 110, F04S10. https://doi.org/10.1029/2004JF000173.
Van Landeghem, K.J.J., Uehara, K., Wheeler, A.J., Mitchell, N.C., Scourse, J.D., 2009a. Postglacial sediment dynamics in the Irish Sea and sediment wave morphology: data-model comparisons. Cont. Shelf Res. 29, 1723–1736. https://doi.org/10.1016/j.csr.2009.05.014.
Van Landeghem, K.J.J., Wheeler, A.J., Mitchell, N.C., Sutton, G., 2009b. Variations in sediment wave dimensions across the tidally dominated Irish Sea, NW Europe. Mar. Geol. 263, 108–119. https://doi.org/10.1016/j.margeo.2009.04.003.
Van Landeghem, K.J.J., Baas, J.H., Mitchell, N.C., Wilcockson, D., Wheeler, A.J., 2012. Reversed sediment wave migration in the Irish Sea, NW Europe: a reappraisal of the validity of geometry-based predictive modelling and assumptions. Mar. Geol. 295, 95–112. https://doi.org/10.1016/j.margeo.2011.12.004.
Van Santen, R.B., De Swart, H.E., Van Dijk, T.A.G.P., 2011. Sensitivity of tidal sand wavelength to environmental parameters: a combined data analysis and modelling approach. Cont. Shelf Res. 31, 966–978. https://doi.org/10.1016/j.csr.2011.03.003.
Walgreen, M., Calvete, D., De Swart, H.E., 2002. Growth of large-scale bed forms due to storm-driven and tidal currents: a model approach. Cont. Shelf Res. 22, 2777–2793. https://doi.org/10.1016/S0278-4343(02)00126-7.
Walker, I.J., 1999. Secondary airflow and sediment transport in the lee of a reversing dune. Earth Surf. Process. Landf. 24, 437–448. https://doi.org/10.1002/(SICI)1096-9837(199905)24:5<437::AID-ESP999>3.0.CO;2-Z.
Walker, I.J., Nickling, W.G., 2002. Dynamics of secondary airflow and sediment transport over and in the lee of transverse dunes. Prog. Phys. Geogr. 26, 47–75. https://doi.org/10.1191/0309133302pp325ra.
Walker, I.J., Nickling, W.G., 2003. Simulation and measurement of surface shear stress over isolated and closely spaced transverse dunes in a wind tunnel. Earth Surf. Process. Landf. 28, 1111–1124. https://doi.org/10.1002/esp.520.
Wasson, R.J., Hyde, R., 1983. Factors determining desert dune type. Nature 304,

337–339. https://doi.org/10.1038/309091a0.
Wienberg, C., Hebbeln, D., 2005. Impact of dumped sediments on subaqueous dunes, outer Weser Estuary, German Bight, southeastern North Sea. Geo-Mar. Lett. 25, 43–53. https://doi.org/10.1007/s00367-004-0202-1.
Wilbers, A., 2004. The Development and Hydraulic Roughness of Subaqueous Dunes. Doctoral Dissertation. Uetrecht Univ., Uetrecht.
Wynn, R.B., Masson, D.G., Bett, B.J., 2002. Hydrodynamic significance of variable ripple morphology across deep-water barchan dunes in the Faroe–Shetland Channel. Mar. Geol. 192, 309–319. https://doi.org/10.1016/S0025-3227(02)00561-3.
Xia, D.X., Wu, S.Y., Liu, Z.X., Yin, P., Qi, F.Q., Ye, Y.C., Xie, Q.C., Chen, X.T., Lai, X.H., Chen, X.L., 2001. Research on the activity of submarine sand waves off Dongfang, Hainan Island. J. Oceanogr. Huanghai Bohai Seas 19, 17–24 (in Chinese).
Xu, Z.W., Wang, Y.P., Li, Y., Ma, F., Zhang, F., Ye, C.J., 2010. Sediment transport patterns in the eastern Beibu Gulf based on grain-size multivariate statistics and provenance analysis. Acta Oceanol. Sin. 32, 67–78 (in Chinese).
Yao, Y.T., Harff, J., Meyer, M., Jan, W.H., 2009. Reconstruction of paleocoastlines for the northwestern South China Sea since the Last Glacial Maximum. Sci. China Ser. D Earth Sci. 52, 1127–1136. https://doi.org/10.1007/s11430-009-0098-8.